

Sub-Cauchy Sampling: Escaping the Dark Side of the Moon

Sebastiano Grazzi¹, Sifan Liu², Gareth O. Roberts³, and Jun Yang⁴

¹Department of Decision Sciences and BIDSA, Bocconi University

²Department of Statistical Science, Duke University

³Department of Statistics, University of Warwick

⁴Department of Mathematical Sciences, University of Copenhagen

Abstract

We introduce a Markov chain Monte Carlo algorithm based on Sub-Cauchy Projection, a geometric transformation that generalizes stereographic projection by mapping Euclidean space into a spherical cap of a hyper-sphere, referred to as the complement of the dark side of the moon¹. We prove that our proposed method is uniformly ergodic for sub-Cauchy targets, namely targets whose tails are at most as heavy as a multidimensional Cauchy distribution, and show empirically its performance for challenging high-dimensional problems. The simplicity and broad applicability of our approach open new opportunities for Bayesian modeling and computation with heavy-tailed distributions in settings where most existing methods are unreliable.

Key words— Heavy-tailed distribution, Metropolis–Hastings, Stereographic MCMC, Geometric projection, Robust Bayesian inference.

1 Introduction

1.1 Sampling heavy-tailed distributions

Heavy-tailed distributions are characterized by tails that decay polynomially rather than exponentially, thereby assigning much larger probabilities to extreme values compared to light-tailed distributions such as the exponential or Gaussian. This class of distributions arises naturally in many fields, including finance, insurance, and climate science, where extreme events occur more frequently and have large impact. For such models, the likelihood is typically heavy-tailed as a function of both the data and the model parameters, which frequently induces a heavy-tailed posterior distribution. Heavy-tailed posteriors also arise in binary regression problems under separation [Gelman et al., 2008, Ghosh et al., 2018] and in robust estimation. As originally noted by De Finetti [1961], for heavy-tailed models, the contribution of extreme observations to the first two moments of the posterior distribution (when they exist) becomes negligible as the observation magnitude increases. This observation was later formalized in a general setting

¹term chosen in homage to Pink Floyd’s *The Dark Side of the Moon* (1973).

within the framework of *Bayesian conflict resolution*, which studies the rather subtle and delicate interplay between prior and likelihood specification in the presence of outliers. See O'Hagan and Pericchi [2012] for a comprehensive review and, e.g., Gagnon and Hayashi [2023], De and Ghosh [2025] and references therein for successful applications of robust Bayesian estimation with heavy-tailed distributions.

Despite these modeling advances, many challenges remain on the computational side. For heavy-tailed posteriors, most popular Metropolis–Hastings algorithms are not geometrically ergodic [Jarner and Hansen, 2000, Livingstone et al., 2019, Wang and Yang, 2025]. For specific statistical models (particularly regression problems), the most popular computational approach is based on Gibbs sampling with an appropriate data augmentation scheme [Polson et al., 2013, Ghosh et al., 2018, Liu, 2004, Gagnon and Hayashi, 2023]. These algorithms can be applied only when simulating from the full conditional distributions is possible, thereby restricting the set of models and priors. Furthermore, convergence guarantees of the Gibbs sampler for heavy-tailed targets are limited and empirical studies suggest slow mixing [Ghosh et al., 2018].

As a consequence, the lack of broadly applicable and reliable sampling methods has limited the use of heavy-tailed models in Bayesian practice, despite their well-recognized statistical advantages. This paper directly addresses this gap by providing a simple, principled, and generally applicable approach for sampling from heavy-tailed posterior distributions.

1.2 Overview of our contributions

At a high level, the proposed Markov chain Monte Carlo (MCMC) algorithm proceeds by first mapping the original state space \mathbb{R}^d onto a spherical cap of a unit sphere, thereby transforming the target distribution on \mathbb{R}^d into a distribution supported on a subset of the sphere. A new random-walk-type Metropolis algorithm is then used to sample the target on the spherical cap, and the resulting samples are mapped back to the original space \mathbb{R}^d via the inverse transformation.

The inverse mapping from the spherical cap to \mathbb{R}^d is termed the *Sub-Cauchy Projection* (SCP). To describe it precisely, we place a d -dimensional unit sphere, which lives in \mathbb{R}^{d+1} , above the d -dimensional hyperplane $\{(y, 0) : y \in \mathbb{R}^d\} \subset \mathbb{R}^{d+1}$. The hyperplane is tangent to the sphere at the origin $(0, \dots, 0) \in \mathbb{R}^{d+1}$, which corresponds to the south pole of the sphere. An *observer* $o \in \mathbb{R}^{d+1}$ is placed *inside* this sphere, and the portion of the spherical surface lying above the observer is removed. The removed spherical cap is hereafter referred to as the *dark side of the moon*, and its complement is called the *bright side*. For a point x on the bright side of the sphere, the Sub-Cauchy Projection $y = \text{SCP}_o(x) \in \mathbb{R}^d$ is defined as the intersection of the line passing through o and x with the hyperplane $\{(y, 0) : y \in \mathbb{R}^d\}$. See Fig. 1 for an illustration with two different choices of the observer o .

For every observer o , the map SCP_o is a smooth and bijective map from the bright side to \mathbb{R}^d (a diffeomorphism), although it does not preserve distances and volumes. When $o = (0, \dots, 0, 2)$, corresponding to the north pole of the sphere, we recover the classical stereographic projection² [see e.g. Coxeter, 1961], and the dark side degenerates to the singleton o . For any other choice of o inside the sphere, however, the Sub-Cauchy Projection differs from the classical stereographic projection in two important ways:

- The dark side is a d -dimensional region, rather than a point, and points at infinity in \mathbb{R}^d are mapped to its $(d - 1)$ -dimensional boundary. This difference is reflected in the Jacobian of the transformation (Remark 1) and enables SCP to accommodate target distributions with heavier tails than those that can be handled by classical stereographic projection (Remark 2).

²Stereographic projection can also be defined with the sphere centered at the origin (see [Yang et al., 2024, Fig. 2]). These two definitions are equivalent up to a rescaling constant.

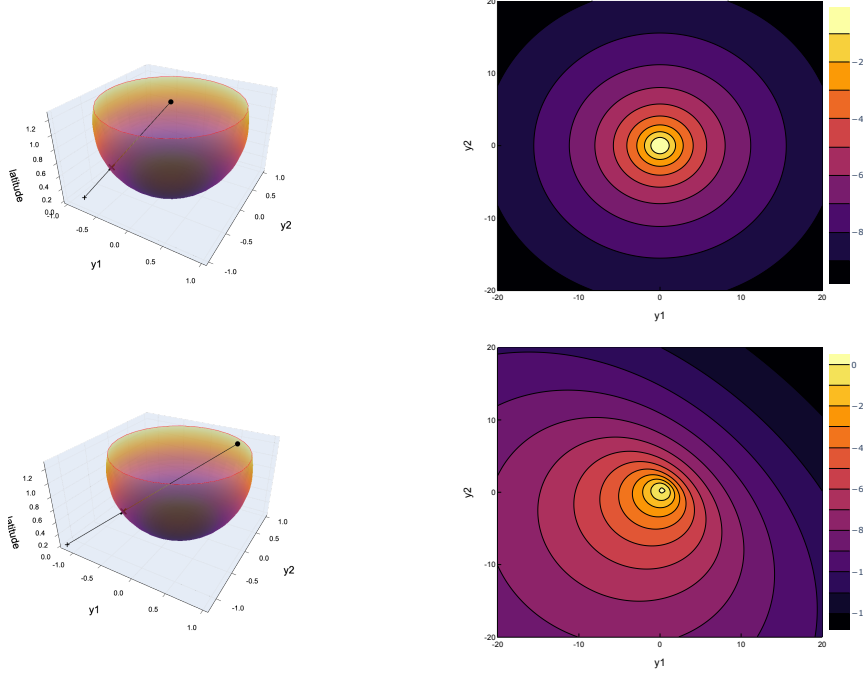


Figure 1: Illustration of a 2-dimensional Sub-Cauchy Projection with $o = (0, 0, 1.5)$ (top panels) and $o = (0.6, 0.6, 1.5)$ (bottom panels). Right panels: contours of log density of the uniform distribution on the bright side of the sphere projected onto \mathbb{R}^2 .

- The observer o acts as a tuning parameter that provides additional flexibility beyond classical stereographic projection. In particular, by varying the location of o , the map SCP_o can be skewed toward certain direction, making it well suited for sampling from asymmetric or skewed heavy-tailed distributions.

Our proposed algorithm, termed the *Sub-Cauchy Projection Sampler* (SCS), is a random-walk-type Metropolis algorithm on the bright side. Our main theoretical result establishes that SCS is *uniformly ergodic* for any d -dimensional *sub-Cauchy distributions*, that is, distributions with tails which are at most as heavy as a d -dimensional Cauchy distribution, see Definition 1. To the best of our knowledge, SCS is the first general-purpose Metropolis-adjusted algorithm with provable uniform ergodicity guarantees for multidimensional sub-Cauchy distributions.

Definition 1. *A distribution π in \mathbb{R}^d is sub-Cauchy if*

$$\sup_{y \in \mathbb{R}^d} \pi(y)(1 + \|y\|^2)^{(d+1)/2} < \infty.$$

Beyond the theoretical guarantees, we provide practical guidelines for selecting the observer parameter o , along with additional tuning parameters such as shifting and rescaling constants. We further demonstrate the performance of SCS on a range of high-dimensional heavy-tailed target distributions, including examples arising from robust Bayesian binary regression, where data-augmentation Gibbs samplers are known to mix slowly [Ghosh et al., 2018]. In these settings, SCS converges much faster, provides more accurate exploration of the posterior tails, and achieves greater computational efficiency than commonly used alternatives such as Hamiltonian Monte Carlo.

1.3 Illustration on the Cauchy distribution

Before going into the details of our method, we present an illustrative example to demonstrate the advantages of SCS and to explain the underlying intuition. We compare the performance

of SCS with other popular MCMC methods for a prototypical example of a heavy-tailed target distribution: the 100-dimensional Cauchy distribution. For this target, the Stereographic Projection Sampler (SPS; Yang et al., 2024, Algorithm 1) and standard MCMC algorithms such as random-walk Metropolis (RWM), Metropolis adjusted Langevin algorithm (MALA), and Hamiltonian Monte Carlo (HMC) fail to be geometrically ergodic [Yang et al., 2024, Jarner and Hansen, 2000, Roberts and Tweedie, 1996, Livingstone et al., 2019], resulting in slow mixing of the corresponding Markov chains. Fig. 2 compares the trajectories of our SCS (with parameters chosen as in Section 3), SPS, together with other popular algorithms such as RWM and HMC. The left panel shows the traces of the squared norm started at stationary and the middle panel shows the first two coordinates when the chains are started at the tails. In the latter case, SPS is stuck at initialization, and we therefore omit its output. The empirical acceptance probability is approximately 0.234 for SCS, SPS and RWM, and 0.7 for HMC, as prescribed by the literature.

There is a simple geometric reason explaining the different behavior of SCS and SPS, with the latter corresponding to SCS when the observer o is placed at the north pole. For the stereographic projection (SP), the transformed density on the surface of the sphere is unbounded near the north pole, because the tails of the multivariate Cauchy density are too heavy. In contrast, for any other choice of o inside the sphere, the density induced by SCP remains bounded on the bright side; see Fig. 3 for an illustration in 2 dimensions. This seemingly subtle difference between the two projections has important consequences: when initialized in the tails, SPS tends to become trapped near the north pole (the dark side of the moon), whereas SCS escapes the dark side and is able to efficiently explore the target distribution.

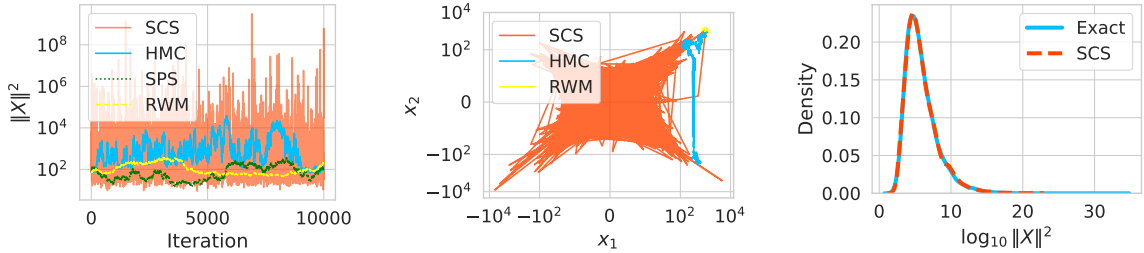


Figure 2: Sampling from a 100-dimensional standard Cauchy distribution. Left panel: trace plot of $\|X\|^2$ of SCS (orange), HMC (blue), SPS (green), and RWM (yellow), initializing from a sample drawn from the target. Middle panel: trajectory in the first two dimensions (on the log scale) of SCS (orange), HMC (blue), and RWM (yellow), initializing from $(10^3, 10^3, \dots)$. Right panel: density of the SCS samples of $\|X\|^2$ (red, estimated by kernel density regression), compared against the true density (blue).

1.4 Related work

Our work overcomes current limitations of popular MCMC methods, which are not geometrically ergodic for heavy-tailed targets [Jarner and Hansen, 2000, Sec. 4] [Livingstone et al., 2019, Thm. 2.2], [Wang and Yang, 2025, Prop. 2]. Some transformation strategies have been proposed to regain geometric/uniform ergodicity [Johnson and Geyer, 2012, Yang et al., 2024], with the former not recovering uniform ergodicity and the latter not suitable for d -dimensional distributions without finite $(d-1)$ -th moment [Yang et al., 2024, Thm 2.1 and Thm 2.2] [Bresar et al., 2025, Sec 3.1.3]. The past years have seen a growing interest in sampling algorithms for heavy-tailed distributions. For example, [He et al., 2022, Mousavi-Hosseini et al., 2023, Vasdekis and Roberts, 2023, He et al., 2024, Bertazzi and Vasdekis, 2025] derived theoretical guarantees

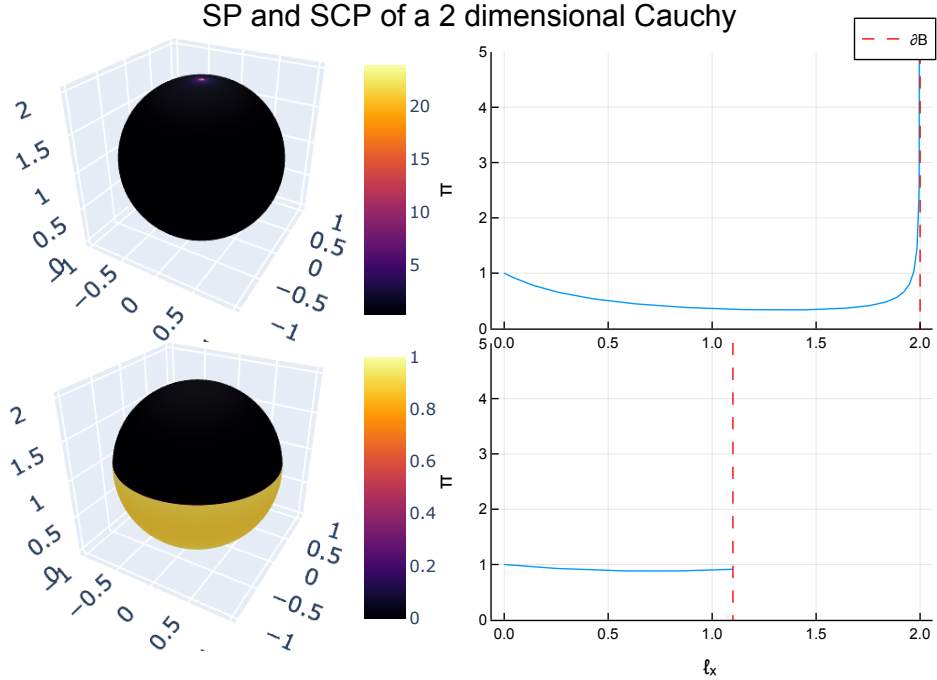


Figure 3: SP (top panels) and SCP with observer $o = (0, 0, 1.1)$ (bottom panels) of 2-dimensional Cauchy distribution. Right panels correspond to the unnormalized density evaluated along the latitude component ℓ_x . The density on the sphere peaks to infinity on the north pole for SP, while it is bounded from above and below for SCP.

for Langevin dynamics and piecewise deterministic Markov processes. However, existing analyses focus either on the continuous time dynamics or the so-called unadjusted setting, which introduces a bias to the target that is difficult to quantify in practical scenarios. Our focus is on Metropolis-adjusted algorithms for heavy-tailed target distributions, for which mostly negative results have been derived [Roberts and Tweedie, 1996, Jarner and Hansen, 2000, Livingstone et al., 2019], although Jarner and Roberts [2007] showed that the use of heavy-tailed MCMC proposal distributions can mitigate slow polynomial rates of convergence to some extent.

1.5 Outline and notation

The remainder of the paper is organized as follows. Section 2.1 provides a detailed description of the Sub-Cauchy Projection. Section 2.2 introduces our proposed algorithm, Sub-Cauchy Projection Sampler (SCS). Section 2.3 establishes the uniform ergodicity of the proposed sampler for sub-Cauchy distributions. Section 3 describes how the tuning parameters of the proposed method are automatically calibrated. Section 4 numerically tests our algorithm for complex heavy-tailed high-dimensional distributions. Code for reproducing the numerical results is available at <https://github.com/liusf15/sub-cauchy-sampler>. More technical proofs are deferred to Appendix A.

Notation. For a vector $z \in \mathbb{R}^{d+1}$, let $h_z := z_{1:d} \in \mathbb{R}^d$ and $\ell_z := z_{d+1} \in \mathbb{R}$ be respectively the horizontal component (longitude) and the vertical component (latitude) of z . For $d \geq 1$ and $s \in \mathbb{R}^{d+1}$, let $\bar{\mathcal{B}}^{d+1}(s) := \{x \in \mathbb{R}^{d+1} : \|x - s\| \leq 1\}$, $\mathcal{S}^d(s) := \{x \in \mathbb{R}^{d+1} : \|x - s\| = 1\}$, and $\mathcal{B}^{d+1}(s) := \bar{\mathcal{B}}^{d+1}(s) \setminus \mathcal{S}^d(s)$. For a fixed $o \in \mathcal{B}^{d+1}(s)$, the bright side of the sphere $\mathcal{S}^d(s)$ is defined as

$$\mathcal{C}_o^d(s) := \{x \in \mathcal{S}^d(s) : x_{d+1} < o_{d+1}\}.$$

When $s = (0, 0, \dots, 0)$, we omit the argument and simply write \mathcal{B}^{d+1} , \mathcal{S}^d , \mathcal{C}_o^d . For all $1 \leq i \leq$

$d+1$, e_i denotes i th standard basis vector in \mathbb{R}^{d+1} .

2 Sampling sub-Cauchy distributions

2.1 Sub-Cauchy Projection

Let the observer be $o \in \mathcal{B}^{d+1}(e_{d+1})$. The d -dimensional Sub-Cauchy Projection $\text{SCP}_o : \mathcal{C}_o^d(e_{d+1}) \rightarrow \mathbb{R}^d$ maps any point $x \in \mathcal{C}_o^d(e_{d+1})$ to $y \in \mathbb{R}^d$ such that x, o , and $\bar{y} = (y, 0) \in \mathbb{R}^{d+1}$ are colinear, that is,

$$x = t o + (1 - t) \bar{y}, \quad \text{for some } t \in [0, 1].$$

By further shifting and rescaling y as $yR + \mu$, where $\mu \in \mathbb{R}^d$ and $R > 0$, we generalize the projection to spheres of radius R centered at (μ, R) . We denote this projection as SCP_θ , where $\theta = (o, \mu, R)$. Explicit expressions of the Sub-Cauchy Projection, its inverse, and its Jacobian are given below. The derivation is provided in Appendix A.1.

Proposition 1. *Fix $\theta = (o, \mu, R)$, where $o \in \mathcal{B}^{d+1}(e_{d+1})$, $\mu \in \mathbb{R}^d$, and $R > 0$. The Sub-Cauchy Projection takes the form*

$$y = \text{SCP}_\theta(x) = R \left(\frac{\ell_o}{\ell_o - \ell_x} h_x - \frac{\ell_x}{\ell_o - \ell_x} h_o \right) + \mu, \quad x \in \mathcal{C}_o^d(e_{d+1}),$$

with inverse

$$\begin{pmatrix} h_x \\ \ell_x \end{pmatrix} = \text{SCP}_\theta^{-1}(y) = \begin{pmatrix} M\hat{y} + (1 - M)h_o \\ (1 - M)\ell_o \end{pmatrix}, \quad \hat{y} = (y - \mu)/R, \quad y \in \mathbb{R}^d,$$

where

$$M = \frac{-\left(\langle \hat{y} - h_o, h_o \rangle - \ell_o(\ell_o - 1)\right) + \sqrt{\left(\langle \hat{y} - h_o, h_o \rangle - \ell_o(\ell_o - 1)\right)^2 - (\|\hat{y} - h_o\|^2 + \ell_o^2)(\|h_o\|^2 + \ell_o^2 - 2\ell_o)}}{\|\hat{y} - h_o\|^2 + \ell_o^2}. \quad (1)$$

The Jacobian of the forward map SCP_θ is

$$J_\theta(y) = R^d \left(\frac{M\|\hat{y} - h_o\|^2 + \langle \hat{y} - h_o, h_o \rangle + \ell_o - \ell_o^2(1 - M)}{M^d \ell_o} \right). \quad (2)$$

The Jacobian greatly simplifies when the observer is centered in its longitudinal component, that is when $h_o = (0, 0, \dots, 0) \in \mathbb{R}^d$, particularly in the two special cases below, where Example 2 is obtained by extending $o \in \mathcal{B}^{d+1}(e_{d+1})$ to also include the boundary point $(0, 0, \dots, 0, 2) \in \mathbb{R}^{d+1}$.

Example 1. (Cauchy projection) If $h_o = (0, 0, \dots, 0) \in \mathbb{R}^d$ and $\ell_o = 1$, then

$$J_\theta(y) = R^d (\|\hat{y}\|^2 + 1)^{(d+1)/2}, \quad \text{where } \hat{y} = (y - \mu)/R. \quad (3)$$

In this case, $J_\theta(y)^{-1}$ is proportional to the density of a standard d -dimensional Cauchy distribution (when $\mu = (0, 0, \dots, 0)$, $R = 1$). Therefore, the inverse of SCP_θ maps the d -dimensional Cauchy distribution into the uniform distribution on the bright side of moon.

Example 2. (Stereographic projection) If $h_o = (0, 0, \dots, 0) \in \mathbb{R}^d$ and $\ell_o = 2$, then we recover the classical stereographic projection with

$$J_\theta(y) = R^d \left(\frac{\|\hat{y}\|^2 + 4}{4} \right)^d, \quad \hat{y} = (y - \mu)/R. \quad (4)$$

Here $J_\theta(y)^{-1}$ is proportional to the density of a standard multivariate student's t with degrees of freedom d (when $\mu = (0, 0, \dots, 0)$, $R = \sqrt{d}/2$).

Remark 1. The inverse of Jacobian in Eq. (3) decays slower than that in Eq. (4) by a factor of $\|\hat{y}\|^{d-1}$ as $\|y\| \rightarrow \infty$. This allows us to improve the uniform ergodicity result in [Yang et al., 2024, Theorem 2.1] for targets that have sub-Cauchy tails.

2.2 Sub-Cauchy Projection Sampler

We detail here our proposed Sub-Cauchy Projection Sampler (SCS). SCS is a random-walk-type Metropolis algorithm on the bright side of the moon. The Metropolis acceptance–rejection ensures that the chain satisfies the detailed-balance condition and is π -invariant. Special care must be taken near the boundaries, as proposals landing on the “dark side” (i.e. above the observer o) are re-located on the the “bright side”, without breaking symmetries and detailed-balance. For simplicity, we define the algorithm on unit spheres centered at 0.

For a given point $x \in \mathcal{S}^d$, a new point x' is first proposed by sampling a Gaussian random variable on the tangent space of the unit sphere at x and projecting it back onto \mathcal{S}^d ; see Algorithm 1. This initial proposal coincides with the SPS proposal in [Yang et al., 2024, Algorithm 1] and allows us to leverage existing theoretical results. If the initial proposed point x' lands on the bright side, we let $x^* = x'$. Otherwise, x' lands in the dark side, i.e., $\ell_{x'} > \ell_o - 1$, we bring it back to the bright side with a *stepping-out* function given by

$$x^* := \cos(K\alpha)x + \sin(K\alpha)u, \quad (5)$$

in which $K := \arg \min_k \{k \in \mathbb{N} : k\alpha > \phi + \gamma\}$, $u := (x' - (\langle x, x' \rangle)x)/\sqrt{1 - (\langle x, x' \rangle)^2}$, $\alpha = \arccos(\langle x, x' \rangle)$, and where $\phi := \arccos(x_{d+1}/\sqrt{x_{d+1}^2 + u_{d+1}^2})$, $\gamma := \arccos(\ell_o - 1/\sqrt{x_{d+1}^2 + u_{d+1}^2})$; see Fig. 4 for an illustration.

Note that the stepping-out step does not incur additional computational cost, since Eq. (5) admits a closed-form expression. Throughout, we set $\ell_o \geq 1$, and we show in Appendix A.4 that for suitable choices of ℓ_o , the initial proposal x' lies on the bright side with high probability as the dimension increases, so that Eq. (5) is invoked only sporadically. The proposed point is then accepted with probability

$$\alpha(y, y^*) = \frac{J_\theta(y^*)\pi(y^*)}{J_\theta(y)\pi(y)} \wedge 1, \quad (6)$$

where y, y^* are respectively x, x^* projected in the Euclidean space via SCP_θ . If the proposed point is rejected, the new state is set to be equal to x ; see Algorithm 2 for the full description of the transition.

As the proposal is symmetric on the sphere and the stepping-out function in Eq. (5) is symmetric relative to the proposal density, SCS satisfies the detailed-balance condition and the following proposition holds true. The proof is provided in Appendix A.2.

Proposition 2. If $\pi(y)$ is positive and continuous in \mathbb{R}^d , then SCS gives rise to an ergodic Markov chain in \mathbb{R}^d with invariant distribution π .

Algorithm 1 Random-walk proposal on unit sphere

Require: Current state $x \in \mathcal{S}^d$, step-size $h > 0$.

- 1: Sample $\tilde{\delta} \sim \mathcal{N}(0, h^2 I_{d+1})$
- 2: Set $\delta = \tilde{\delta} - \langle x, \tilde{\delta} \rangle x$
- 3: **return** $x' = \frac{x + \delta}{\|x + \delta\|}$

Algorithm 2 Sub-Cauchy Projection Sampler (SCS) transition (on unit sphere)

Require: Current state $x \in \mathcal{S}^d$, tuning parameters $\theta = (o, R, \mu)$, step-size $h > 0$.

- 1: Propose $x' \in \mathcal{S}^d$ with Algorithm 1.
- 2: If $\ell_{x'} > \ell_o - 1$ (x' is in dark side), set x^* as in Eq. (5), otherwise set $x^* = x'$.
- 3: Compute $\alpha(y, y^*)$ as in Eq. (6), where $y = \text{SCP}_\theta(x + e_{d+1})$, $y^* = \text{SCP}_\theta(x^* + e_{d+1})$
- 4: With probability $\alpha(y, y^*)$, set $x^{\text{new}} = x^*$; otherwise set $x^{\text{new}} = x$.
- 5: **return** next state x^{new} .

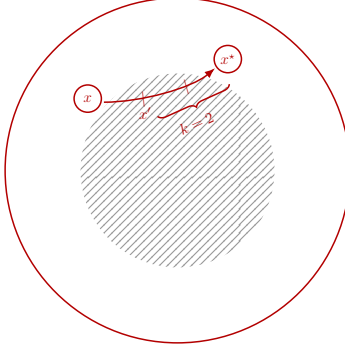


Figure 4: Top view of the stepping-out mechanism. The shaded area represents the dark side. Starting from x , the point x' was proposed in the dark side and the stepping-out function bring it back to the bright-side x^* .

2.3 Uniform Ergodicity

Our main result shows that the convergence of the SCS chain to a sub-Cauchy target π is exponential, and its speed does not depend on the starting value. Formally, a Markov chain is *uniformly ergodic* if, for all $y \in \mathbb{R}^d$,

$$\|\mathcal{P}^n(y, \cdot) - \pi\| \leq C\rho^n,$$

for some constants $C > 0$, $0 < \rho < 1$, where $\|\cdot\|$ denotes total variation distance and $\mathcal{P}^n(y, \cdot)$ denotes the law of the Markov chain initialized at y after n steps. Uniform ergodicity is a strong (yet qualitative) property that is rarely satisfied for Metropolis–Hastings chains in \mathbb{R}^d .

Theorem 1. *If $\pi(y)$ is positive and continuous on \mathbb{R}^d , then SCS with any fixed $\ell_o \in [1, 2)$ is uniformly ergodic if and only if*

$$\sup_{y \in \mathbb{R}^d} \pi(y) J_\theta(y) < \infty,$$

where $J_\theta(y)$ is given in Eq. (2).

Theorem 1 implies that the proposed SCS is uniformly ergodic for a large class of heavy/light-tailed distributions, including distributions with tails no heavier than a (multivariate) Cauchy distribution; see Corollary 1. To the best of our knowledge, SCS is the first general-purpose Metropolis-adjusted MCMC with such provable convergence guarantees.

Corollary 1 (Uniform ergodicity of SCS for sub-Cauchy distributions). *If $\pi(y)$ is sub-Cauchy, positive and continuous in \mathbb{R}^d , then SCS with any fixed $\ell_o \in [1, 2)$ is uniformly ergodic.*

Proof. By Theorem 1, it suffices to show $\sup_{y \in \mathbb{R}^d} \pi(y) J_\theta(y) < \infty$. Since

$$\sup_{y \in \mathbb{R}^d} \pi(y) J_\theta(y) \leq \left[\sup_{y \in \mathbb{R}^d} \pi(y) (1 + \|y\|^2)^{(d+1)/2} \right] \cdot \left[\sup_{y \in \mathbb{R}^d} (1 + \|y\|^2)^{-(d+1)/2} J_\theta(y) \right],$$

and the first term is finite by Definition 1, it suffices to show

$$\sup_{y \in \mathbb{R}^d} (1 + \|y\|^2)^{-(d+1)/2} J_\theta(y) < \infty.$$

As R, μ , and $\ell_o < 2$ are constants, this is verified by substituting $J_\theta(y)$ in Eq. (2), using the continuity of π , and taking the limit as $\|y\| \rightarrow \infty$. \square

Remark 2. *Corollary 1 offers a substantial improvement to the uniform ergodicity result of SPS in Yang et al. [2024, Theorem 2.1], which holds only for d -dimensional targets with lighter tails than a student's t with degree of freedom $\nu \geq d$. In particular, SPS is not geometrically ergodic for student's t with $\nu < d$ [Yang et al., 2024, Proof of Theorem 2.1]/[Brešar et al., 2025, Sec. 3.1.3]; see also the numerical comparison in Section 1.3.*

3 Tuning parameters

In this section, we provide a principled approach to select the tuning parameters of SCP before running the MCMC algorithm. For a given latitude of the observer $\ell_o \in [1, 2)$, the goal is to choose the parameter $\bar{\theta} = (h_o, \mu, R)$ such that the target π transformed to the bright side $\mathcal{C}_o^d(e_{d+1})$ is close to the uniform distribution. This is because when the density on the bright side is uniform, Algorithm 2 has acceptance probability equal to 1 for any step-size $h > 0$, leading to fast mixing and small auto-correlation.

Throughout, the latitude ℓ_o is fixed (see Appendix A.4 for guidance motivated by simple geometric arguments), while the step-size $h > 0$ of SCS is tuned in order to achieve a certain average empirical acceptance probability [Gelman et al., 1996, Roberts et al., 1997], leaving the total number of iterations as the only user-specified parameter.

Remark 3. *Popular adaptive schemes for tuning MCMC hyperparameters [e.g. Gilks et al., 1998, Bell et al., 2024] are based on estimating and matching the first two moments of the target distribution. This strategy may fail for heavy-tailed distributions, as these distributions do not necessarily have finite moments.*

For a given $\ell_o \in [1, 2)$, let $\bar{\theta} := (h_o, \mu, R) \in \Theta$ where $\Theta = \{h_o \in \mathbb{R}^d : \|h_o\|_2^2 + (\ell_o - 1)^2 \leq 1\} \times \mathbb{R}^d \times \mathbb{R}^+$. Let $q_{\bar{\theta}}$ denote the distribution of $y = \text{SCP}_{\bar{\theta}}(x)$, where $x \sim \text{Unif}(\mathcal{C}_o^d(e_{d+1}))$ and $\theta = (\ell_o, \bar{\theta})$. We optimize $\bar{\theta}$ by minimizing the Kullback-Leibler (KL) divergence between $q_{\bar{\theta}}$ and π , that is, $\min_{\bar{\theta} \in \Theta} \text{KL}(q_{\bar{\theta}} \|\pi)$. This approach falls within the framework of variational inference [Blei et al., 2017], where one seeks to approximate the target π by a distribution from the variational family $\{q_{\bar{\theta}} : \bar{\theta} \in \Theta\}$.

The objective function can be expressed as

$$\begin{aligned} \text{KL}(q_{\bar{\theta}} \|\pi) &= \mathbb{E}_{q_{\bar{\theta}}} [\log q_{\bar{\theta}}(y) - \log \pi(y)] \\ &= \mathbb{E}_{\text{Unif}(\mathcal{C}_o^d(e_{d+1}))} [\log q_{\bar{\theta}}(\text{SCP}_{\bar{\theta}}(x)) - \log \pi(\text{SCP}_{\bar{\theta}}(x))] \\ &= \mathbb{E}_{\text{Unif}(\mathcal{C}_o^d(e_{d+1}))} [-\log J_\theta(x) - \log \pi(\text{SCP}_{\bar{\theta}}(x))]. \end{aligned} \tag{7}$$

The expectation in the objective function can be approximated using Monte Carlo samples drawn from $\text{Unif}(\mathcal{C}_o^d(e_{d+1}))$. The parameter $\bar{\theta}$ is then optimized via stochastic gradient descent, with gradients computed by automatic differentiation, following standard practice in black-box variational inference [Ranganath et al., 2014].

If the target π belongs to the variational family, then SCP with the optimal $\bar{\theta}$ exactly transforms π to the uniform distribution on the bright side $\mathcal{C}_o^d(e_{d+1})$. When π does not lie in the variational family, the induced density on the bright side will not be exactly uniform. Nevertheless, the location parameter μ and scale parameter R allow the variational approximation to

capture the bulk of the target distribution, while the observer o provides an additional degree of freedom to accommodate skewness. The scale parameter R can also be generalized to allow for different scales for different dimensions, although we do not pursue this extension in the present paper. We provide an illustration of the performance of the variational approximation in Section 4.1.

4 Numerical simulations

4.1 Multivariate skew t distribution

We consider here the multivariate skew t distribution introduced by [Branco and Dey, 2001, Azzalini and Capitanio, 2003]. Following Azzalini and Capitanio [2003], a d -dimensional skew t distribution with location $\xi \in \mathbb{R}^d$, scale matrix $\Omega \in \mathbb{R}^{d \times d}$, skewness $\alpha \in \mathbb{R}^d$, and degree of freedom ν can be represented as the distribution of $\xi + V^{-1/2}Z$, where $V \sim \chi_\nu^2/\nu$, and Z follows a skew normal distribution with density

$$2\varphi_d(z; 0, \Omega) \Phi(\alpha^\top \omega^{-1} z),$$

with $\omega = \text{diag}(\Omega_{11}^{1/2}, \dots, \Omega_{dd}^{1/2})$ and where Φ denotes the standard Normal cumulative distribution function and $\varphi_d(y; \mu, \Sigma)$ denotes the d -dimensional Gaussian density with mean μ and variance Σ evaluated at y . We fix $d = 100$, $\xi = \mathbf{0}$, $\Omega = I_d$, and $\alpha = (100, -100, 0, \dots, 0)$. We compare SCS (with latitude $\ell_o = 1.1$ and step-size $h = 0.1$ on the sphere) against the standard HMC sampler, which takes 10 leapfrog steps of size 0.1 in each iteration. Both samplers are initialized at $(1, \dots, 1)$, run for 500,000 iterations, discard the first 100 samples, and retain every 50th sample for evaluation. The average acceptance rates are about 0.4 for SCS and 0.8 for HMC. We compute empirical marginal quantiles at probabilities 0.01, 0.02, 0.05, 0.1, 0.2, 0.5, 0.8, 0.9, 0.95, 0.98, 0.99, and compare them against the corresponding exact quantiles, estimated from 10^7 independent samples directly drawn from the target distribution.

Fig. 5 displays Q–Q plots for the first four coordinates, with variability across 10 independent replicates indicated by the shaded regions. When $\nu = 2$ (top panels), both samplers capture the bulk of the distribution, though HMC is less accurate at the extreme tails. When $\nu = 1$ (bottom panels), corresponding to the skew Cauchy distribution, HMC fails to explore the distribution, whereas SCS continues to perform well, with accurate quantiles up to the 1st and 99th percentiles. Notably, SCS is gradient-free, while HMC requires 10 gradient evaluations per iteration, making SCS much more efficient.

To assess the performance of the variational method described in Section 3, we report the cosine between h_o and α , as well as the relative difference between μ and ξ . In the target distribution, α and ξ respectively control skewness and location. Their counterparts in the variational family are $-h_o$ and μ , which play analogous roles. Hence, we expect h_o and α to become aligned and μ to get close to ξ when using the variational method of Section 3.

In this experiment, we fix $d = 100, \nu = 2$. We use the same α as before, and set the elements of ξ to be equally spaced between -10 and 10 . Optimization of the KL divergence Eq. (7) is carried out with a Monte Carlo sample size of 2000 and the Adam optimizer [Kingma, 2014] with a learning rate of 0.01. As shown in Fig. 6, $\cos(h_o, \alpha)$ approaches -1 as the number of gradient descent steps increases, while $\|\mu - \xi\|_2/\|\xi\|_2$ approaches 0.

To further examine the transient behavior, Fig. 7 shows the trace plots of a single chain from each sampler, both initialized from a cold start at $(500, \dots, 500)$, with $d = 10$ and $\nu = 2$. HMC fails to reach the typical set and continues to wander in the heavy-tailed region even after 100,000 iterations, whereas SCS rapidly converges to the typical set. This illustrates the substantial advantage of SCS over HMC when the chain is initialized far in the tail.

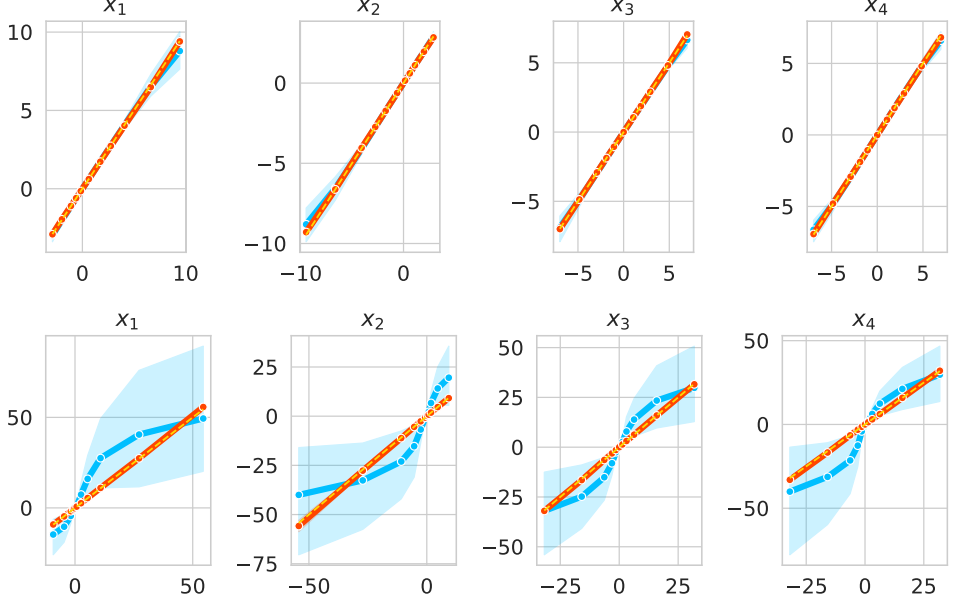


Figure 5: Q–Q plot of SCS (red) and HMC (blue) in sampling a 100-dimensional multivariate skew t distribution with 2 (top) or 1 (bottom) degrees of freedom. Shaded regions show variation across 10 independent replicates.

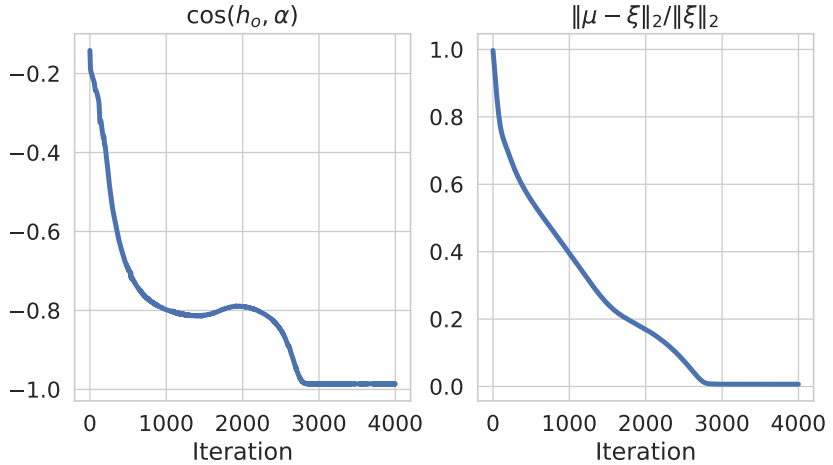


Figure 6: Cosine between h_o and α (left) and relative squared distance between μ and ξ (right) versus the number of gradient descent iterations when optimizing the KL divergence (7).

4.2 Robust Bayesian binary regression

We consider here Bayesian binary regression problems, where the binary response $y_i \in \{0, 1\}$ is modeled as

$$\mathbb{P}(y_i = 1 \mid x_i, \beta) = F(x_i^\top \beta), \quad 1 \leq i \leq n,$$

with covariates $x_i \in \mathbb{R}^d$ and regression coefficients $\beta \in \mathbb{R}^d$. This formulation reduces to the logistic regression model when $F(x) = \frac{1}{1+e^{-x}}$, and to the probit model when $F = \Phi$ is the CDF of the standard normal distribution. Both models are known to be sensitive to outliers, motivating the use of heavier-tailed link functions such as the CDF of a student's t distribution [Albert and Chib, 1993, Liu, 2004], which is known as robit regression. When β has a normal

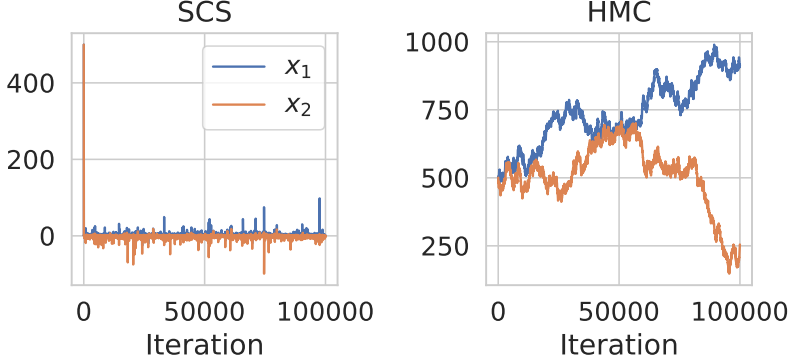


Figure 7: Trace plots of the first two coordinates of SCS (left) and HMC (right) in sampling a 10-dimensional multivariate skew t distribution with 2 degrees of freedom.

prior, geometric ergodicity has been established under suitable conditions for a Gibbs sampler with data augmentation (DA-Gibbs) [Roy, 2012, Mukherjee et al., 2023].

Gelman et al. [2008] propose to use independent t distributions as the default prior for the regression coefficients in logistic regression and other generalized linear models (e.g., multinomial logit and probit). Such priors encode weak prior information and, importantly, stabilize the estimates when the responses are linearly separable. More recently, Ghosh et al. [2018] establish necessary and sufficient conditions for the existence of posterior means under Cauchy priors, and develop a DA-Gibbs for logistic regressions with Cauchy priors.

However, Ghosh et al. [2018] report extremely slow mixing of DA-Gibbs with heavy-tailed priors in the presence of separation. While they acknowledge that alternative samplers such as the No-U-Turn Sampler (NUTS; [Hoffman et al., 2014]) can improve mixing, they note that “the problematic issue of posteriors with extremely heavy tails under Cauchy priors cannot be resolved without altering the prior.” In Appendix A.5, we describe DA-Gibbs under data separation and provide an heuristic argument showing slow-mixing of the chain. In particular, we show that, as $n \rightarrow \infty$, the posterior standard deviation of β is of order $O(\sqrt{n \log n})$, while the DA-Gibbs step-size is of order $O(\sqrt{\log n})$ near the mode. As a result, the step-size is much smaller than the bulk of the posterior distribution, causing high autocorrelation and slow mixing.

We demonstrate the performance of the proposed SCS on the Bayesian logistic regression when there is separation in the data. We set $d = 20$ and $n = 50$. The covariates x_i are generated i.i.d. from the standard normal, and responses are set as $y_i = \mathbf{1}\{x_{i,1} > 0\}$, making the data separable along the first covariate. We consider both logit link and robit link (student’s t with 2 degrees of freedom) in the binary regression. We use the default prior proposed in Gelman et al. [2008], where we first normalize the covariates to have mean 0 and standard deviation 0.5, and then place independent student t priors with scale 2.5. We compare three samplers: SCS (with $\ell_o = 1.1$), Gibbs sampler with data augmentation, and vanilla HMC. For HMC, every iteration runs 10 leapfrog steps, with the step-size tuned to target an average acceptance rate of 0.8. All methods are repeated 20 times independently. Each chain is run for 100 iterations as warm-up. SCS and Gibbs are run for 5,000,000 iterations, while HMC is run for 1,000,000 iterations, keeping the wall-clock time roughly on the same order. After thinning, each chain retain 10,000 samples to calculate the quantiles. Reference quantiles are obtained from NUTS using 20 parallel chains, each with 5,000,000 iterations.

We report the Q–Q plots for β_1 sampled by the three algorithms for the logistic regression (Fig. 8) and robit regression (Fig. 9). The shaded bands indicate variability across 20 independent chains of each method. Consistent with the observation in Ghosh et al. [2018], Gibbs

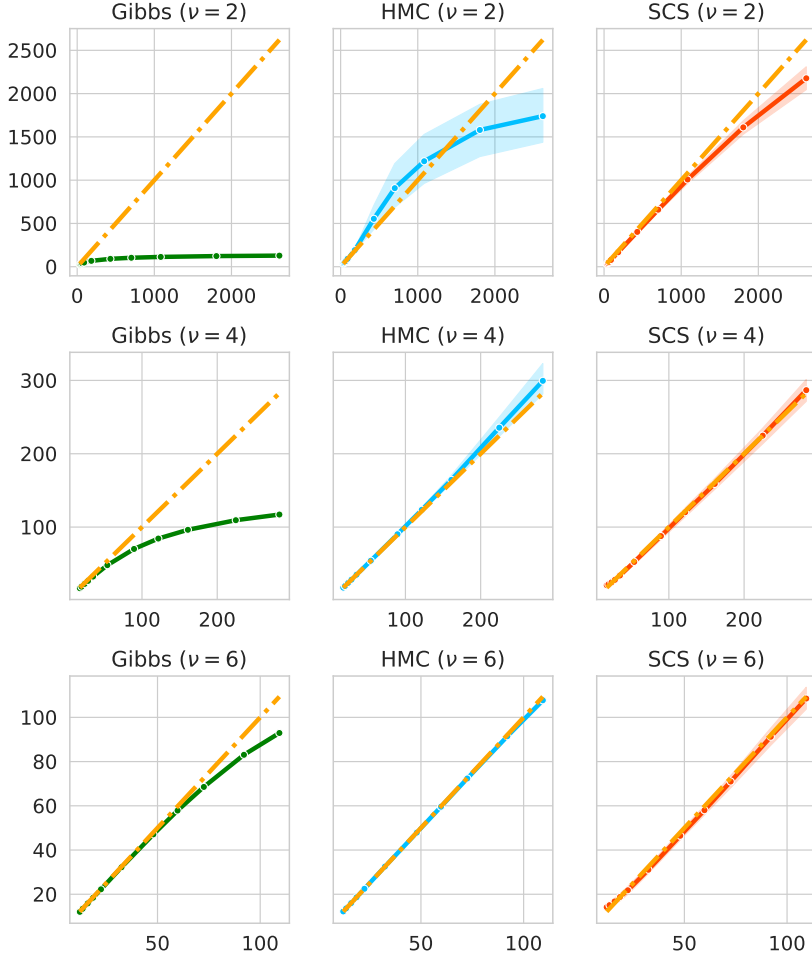


Figure 8: Q–Q plot of β_1 in logistic regression derived with the Gibbs sampler (left columns), HMC (middle column) and SCS (right column). The prior is the t distribution with degree of freedom equal to 2 (top), 4 (middle), or 6 (bottom).

performs poorly when the prior is heavy-tailed, but the performance improves as the degree of freedom increases. HMC is more accurate when $\nu = 4$ or 6 , but struggles to sample in the tail when $\nu = 2$. The proposed SCS method performs more reliably even in the extremely heavy-tailed situations.

5 Discussion

We introduce a new Metropolis–Hastings algorithm, Sub-Cauchy Projection Sampler, that is uniformly ergodic for sub-Cauchy target distributions. The tuning parameters of the projection are automatically set via the variational method, making the proposed SCS broadly applicable whenever the posterior is suspected to be heavy-tailed. Our numerical experiments show that SCS outperforms several popular methods in these scenarios. We conclude the paper by outlining several open problems and directions for future research.

1. *Optimal scaling and adaptive MCMC*: we proposed a variational approach for selecting tuning parameters that works well across our simulations. However, the optimality of this tuning rule remains an open question. A popular framework to adaptively tune hyperparameters in Metropolis–Hastings algorithms is given by the optimal scaling theory [Roberts et al., 1997]. However, in our framework with heavy-tailed targets and geometri-

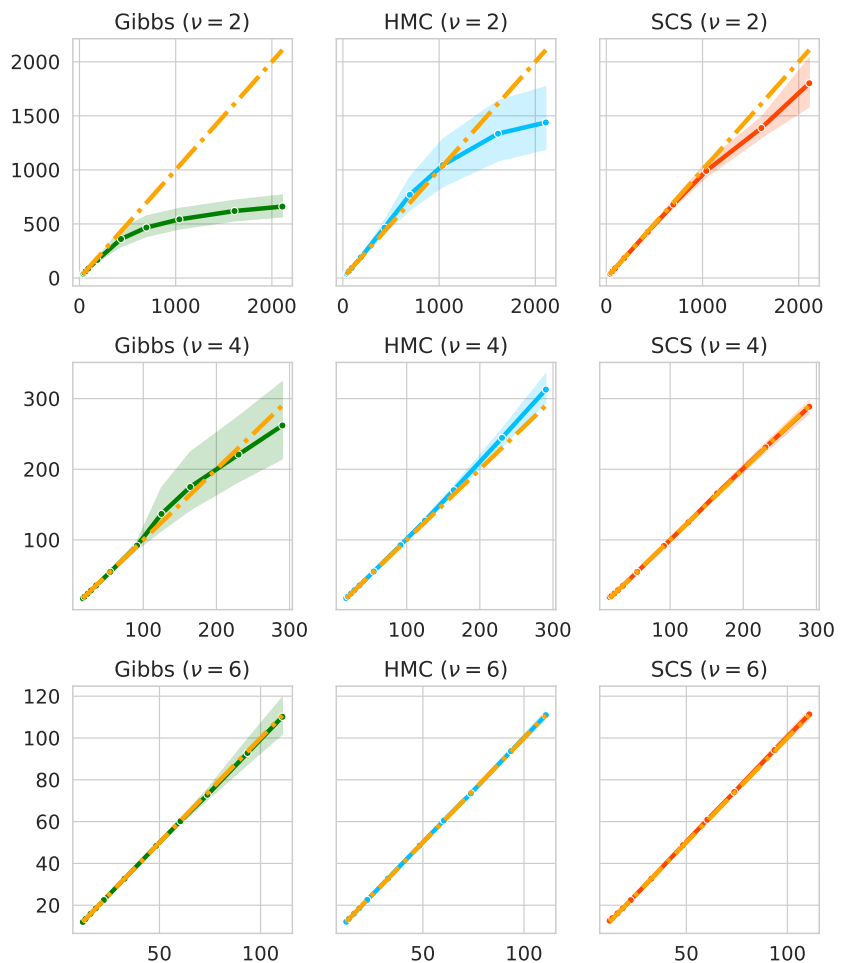


Figure 9: Q–Q plot of β_1 in the robit regression. Caption as in Fig. 8.

cally transformed MCMC algorithms, the derivation of scaling limits is challenging [Yang et al., 2020, 2024]. We therefore defer a rigorous treatment of this issue to future work.

2. *Quantitative convergence results*: Quantitative bounds on the mixing time of MCMC algorithms and their dependence on the dimension have been an active area of theoretical research in recent years [Dwivedi et al., 2019, Chen et al., 2020, Yang and Rosenthal, 2023, Andrieu et al., 2024, Milinanni et al., 2026]. An important direction for future work is to establish rapid mixing guarantees for SCS over a broad class of sub-Cauchy target distributions.
3. *Gradient-based MCMC for sub-Cauchy distributions*: SCS is a random-walk-type algorithm that does not exploit gradient information of the target distribution. An important direction for future work is to integrate SCS with ideas from robust gradient-based MCMC methods [Livingstone and Zanella, 2022, Bell et al., 2026], or to combine it with MCMC frameworks incorporating boundary conditions [Bierkens et al., 2023a,b].

Acknowledgement

The authors would like to thank Nicolas Chopin for helpful discussions on Bayesian robust regression and Wenkai Xu for helpful discussions at the early stage of this work. SG acknowledges support from the European Union (ERC), through the Starting Grant ‘PrSc-HDBayLe’, project number 101076564. JY’s research is supported by the Independent Research Fund Denmark (DFF) through the Sapere Aude Starting Grant (5251-00032B). GOR was supported by PINCODE (EP/X028119/1), EP/V009478/1 and by the UKRI grant, OCEAN, EP/Y014650/1.

References

J. H. Albert and S. Chib. Bayesian analysis of binary and polychotomous response data. *Journal of the American Statistical Association*, 88(422):669–679, 1993.

C. Andrieu, A. Lee, S. Power, and A. Q. Wang. Explicit convergence bounds for Metropolis Markov chains: Isoperimetry, spectral gaps and profiles. *The Annals of Applied Probability*, 34(4):4022–4071, 2024.

A. Azzalini and A. Capitanio. Distributions generated by perturbation of symmetry with emphasis on a multivariate skew t-distribution. *Journal of the Royal Statistical Society Series B: Statistical Methodology*, 65(2):367–389, 2003.

C. Bell, K. Łatuszyński, and G. O. Roberts. Adaptive stereographic MCMC. *arXiv preprint arXiv:2408.11780*, 2024.

C. Bell, J. Yang, K. Łatuszyński, G. O. Roberts, and J. S. Rosenthal. Stereographic Barker’s MCMC proposal: Efficiency and robustness at your disposal. *manuscript in preparation*, 2026.

A. Bertazzi and G. Vasdekis. Sampling with time-changed Markov processes. *arXiv preprint arXiv:2501.15155*, 2025.

J. Bierkens, S. Grazzi, F. v. d. Meulen, and M. Schauer. Sticky PDMP samplers for sparse and local inference problems. *Statistics and Computing*, 33(1):8, 2023a.

J. Bierkens, S. Grazzi, G. Roberts, and M. Schauer. Methods and applications of PDMP samplers with boundary conditions, 2023b. URL <https://arxiv.org/abs/2303.08023>.

D. M. Blei, A. Kucukelbir, and J. D. McAuliffe. Variational inference: A review for statisticians. *Journal of the American statistical Association*, 112(518):859–877, 2017.

M. D. Branco and D. K. Dey. A general class of multivariate skew-elliptical distributions. *Journal of Multivariate Analysis*, 79(1):99–113, 2001.

M. Brešar, A. Mijatović, and G. Roberts. Central limit theorem for ergodic averages of Markov chains & the comparison of sampling algorithms for heavy-tailed distributions. *arXiv preprint arXiv:2512.18255*, 2025.

Y. Chen, R. Dwivedi, M. J. Wainwright, and B. Yu. Fast mixing of Metropolized Hamiltonian Monte Carlo: Benefits of multi-step gradients. *Journal of Machine Learning Research*, 21(92):1–72, 2020.

H. S. M. Coxeter. *Introduction to Geometry*. 1961.

S. De and J. Ghosh. Robust Bayesian model averaging for linear regression models with heavy-tailed errors. *Journal of Applied Statistics*, pages 1–27, 2025. Publisher: Taylor & Francis.

B. De Finetti. The Bayesian approach to the rejection of outliers. In *Proceedings of the 4th Berkeley Symposium on Mathematical Statistics and Probability*, volume 1, pages 99–210. University of California Press Berkeley, CA, USA, 1961.

R. Dwivedi, Y. Chen, M. J. Wainwright, and B. Yu. Log-concave sampling: Metropolis-Hastings algorithms are fast. *Journal of Machine Learning Research*, 20(183):1–42, 2019.

P. Gagnon and Y. Hayashi. Theoretical properties of Bayesian student-t linear regression. *Statistics & Probability Letters*, 193:109693, 2023.

A. Gelman, G. O. Roberts, and W. R. Gilks. Efficient Metropolis jumping rules. *Bayesian Statistics 5*, 5:599–608, 1996.

A. Gelman, A. Jakulin, M. G. Pittau, and Y.-S. Su. A weakly informative default prior distribution for logistic and other regression models. *The Annals of Applied Statistics*, 2(4):1360, 2008.

J. Ghosh, Y. Li, and R. Mitra. On the use of Cauchy prior distributions for Bayesian logistic regression. *Bayesian Analysis*, 13(2):359–383, 2018.

W. R. Gilks, G. O. Roberts, and S. K. Sahu. Adaptive Markov chain Monte Carlo through regeneration. *Journal of the American Statistical Association*, 93(443):1045–1054, 1998.

Y. He, K. Balasubramanian, and M. A. Erdogdu. Heavy-tailed sampling via transformed unadjusted Langevin algorithm. *arXiv preprint arXiv:2201.08349*, 2022.

Y. He, T. Farghly, K. Balasubramanian, and M. A. Erdogdu. Mean-square analysis of discretized itô diffusions for heavy-tailed sampling. *Journal of Machine Learning Research*, 25(43):1–44, 2024.

M. D. Hoffman, A. Gelman, et al. The No-U-Turn sampler: adaptively setting path lengths in Hamiltonian Monte Carlo. *Journal of Machine Learning Research*, 15(1):1593–1623, 2014.

S. F. Jarner and E. Hansen. Geometric ergodicity of Metropolis algorithms. *Stochastic processes and their applications*, 85(2):341–361, 2000.

S. F. Jarner and G. O. Roberts. Convergence of heavy-tailed Monte Carlo Markov chain algorithms. *Scandinavian Journal of Statistics*, 34(4):781–815, 2007.

J. E. Johndrow, A. Smith, N. Pillai, and D. B. Dunson. MCMC for imbalanced categorical data. *Journal of the American Statistical Association*, 2019.

L. T. Johnson and C. J. Geyer. Variable transformation to obtain geometric ergodicity in the random-walk Metropolis algorithm. *The Annals of Statistics*, pages 3050–3076, 2012.

D. P. Kingma. Adam: A method for stochastic optimization. *arXiv preprint arXiv:1412.6980*, 2014.

C. Liu. Robit regression: a simple robust alternative to logistic and probit regression. *Applied Bayesian Modeling and Casual Inference from Incomplete-Data Perspectives*, pages 227–238, 2004.

S. Livingstone and G. Zanella. The Barker proposal: Combining robustness and efficiency in gradient-based MCMC. *Journal of the Royal Statistical Society Series B: Statistical Methodology*, 84(2):496–523, 2022.

S. Livingstone, M. Betancourt, S. Byrne, and M. Girolami. On the geometric ergodicity of Hamiltonian Monte Carlo. *Bernoulli*, 25(4A):3109–3138, 2019.

S. P. Meyn and R. L. Tweedie. *Markov Chains and Stochastic Stability*. Springer Science & Business Media, 2012.

F. Milinanni, T. Farghly, and J. Yang. Rapid mixing of stereographic MCMC for heavy-tailed sampling. *manuscript in preparation*, 2026.

A. Mousavi-Hosseini, T. K. Farghly, Y. He, K. Balasubramanian, and M. A. Erdogdu. Towards a complete analysis of Langevin Monte Carlo: Beyond Poincaré inequality. In *The Thirty Sixth Annual Conference on Learning Theory*, pages 1–35. PMLR, 2023.

S. Mukherjee, K. Khare, and S. Chakraborty. Convergence properties of data augmentation algorithms for high-dimensional robit regression. *Electronic Journal of Statistics*, 17(1):19–69, 2023.

A. B. Owen. Infinitely imbalanced logistic regression. *Journal of Machine Learning Research*, 8(4), 2007.

A. O’Hagan and L. Pericchi. Bayesian heavy-tailed models and conflict resolution: A review. *Brazilian Journal of Probability and Statistics*, 26(4):372 – 401, 2012. doi: 10.1214/11-BJPS164. URL <https://doi.org/10.1214/11-BJPS164>.

N. G. Polson, J. G. Scott, and J. Windle. Bayesian inference for logistic models using pólya–Gamma latent variables. *Journal of the American Statistical Association*, 108(504):1339–1349, 2013.

R. Ranganath, S. Gerrish, and D. Blei. Black box variational inference. In *Artificial Intelligence and Statistics*, pages 814–822. PMLR, 2014.

G. O. Roberts and A. F. Smith. Simple conditions for the convergence of the Gibbs sampler and Metropolis-Hastings algorithms. *Stochastic Processes and their Applications*, 49(2):207–216, 1994.

G. O. Roberts and R. L. Tweedie. Geometric convergence and central limit theorems for multidimensional Hastings and Metropolis algorithms. *Biometrika*, 83(1):95–110, 1996.

G. O. Roberts, A. Gelman, and W. R. Gilks. Weak convergence and optimal scaling of random walk Metropolis algorithms. *The Annals of Applied Probability*, 7(1):110–120, 1997.

V. Roy. Convergence rates for MCMC algorithms for a robust Bayesian binary regression model. *Electronic Journal of Statistics*, 6:2463–2485, 2012.

L. Tierney. Markov chains for exploring posterior distributions. *The Annals of Statistics*, 22(4):1701–1728, 1994.

G. Vasdekis and G. O. Roberts. Speed up zig-zag. *The Annals of Applied Probability*, 33(6A):4693–4746, 2023.

Z. Wang and J. Yang. Stereographic multi-try Metropolis algorithms for heavy-tailed sampling. *arXiv preprint arXiv:2505.12487*, 2025.

J. Yang and J. S. Rosenthal. Complexity results for MCMC derived from quantitative bounds. *The Annals of Applied Probability*, 33(2):1459–1500, 2023.

J. Yang, G. O. Roberts, and J. S. Rosenthal. Optimal scaling of random-walk Metropolis algorithms on general target distributions. *Stochastic Processes and their Applications*, 130(10):6094–6132, 2020.

J. Yang, K. Łatuszyński, and G. O. Roberts. Stereographic Markov chain Monte Carlo. *The Annals of Statistics*, 52(6):2692–2713, 2024.

A Appendix

A.1 Sub-Cauchy Projection and Jacobian determinant

For a fixed observer $o = (h_o, \ell_o) \in \mathcal{B}^{d+1}(e_{d+1}) \subset \mathbb{R}^{d+1}$, a point on the surface of the unit sphere $x = (h_x, \ell_x) \in \mathcal{C}^{d+1}(e_{d+1}) \subset \mathbb{R}^{d+1}$ and rescaling factors $R > 0$, $\mu \in \mathbb{R}^d$, let $\hat{y} = (y - \mu)/R$ be the rescaled point on the plane. The forward map

$$y = \text{SCP}_\theta(x) = R \left(\frac{\ell_o}{\ell_o - \ell_x} h_x - \frac{\ell_x}{\ell_o - \ell_x} h_o \right) + \mu, \quad h_x = x_{1d}, \ell_x = x_{d+1},$$

is simply derived as the straight line connecting o , x and $(\hat{y}, 0)$. To find the inverse map, we use that

$$\begin{pmatrix} h_x \\ \ell_x - 1 \end{pmatrix} = M \begin{pmatrix} \hat{y} \\ -1 \end{pmatrix} + (1 - M) \begin{pmatrix} h_o \\ \ell_o - 1 \end{pmatrix},$$

for some $M \in [0, 1]$. Since $\|h_x\|^2 + (\ell_x - 1)^2 = 1$, by taking the squared norm on both sides of the equation above, we have that

$$1 = M^2 (\|\hat{y} - h_o\|^2 + \ell_o^2) + \|h_o\|^2 + (\ell_o - 1)^2 + 2M (\langle \hat{y} - h_o, h_o \rangle - \ell_o(\ell_o - 1))$$

which has one positive solution M that can be written explicitly in terms of y, o, ℓ_o and R (see (1)). Hence the *inverse map* takes the form

$$\begin{pmatrix} h_x \\ \ell_x \end{pmatrix} = [\text{SCP}_\theta^{-1}(y)] = \begin{pmatrix} M\hat{y} + (1 - M)h_o \\ (1 - M)\ell_o \end{pmatrix}.$$

Let us derive the Jacobian determinant for the map $y = \pi_o(x)$. Let $\bar{y} = (\hat{y}, 0)$, θ_1 be the angle between $\bar{y} - o$ and $x - e_{d+1}$, θ_2 be the angle between $o - \bar{y}$ and e_{d+1} , $a = \|x - o\|$ and $b = \|\bar{y} - x\|$. Then, the Jacobian determinant is defined as

$$\begin{aligned} J(y) &= R^d \left(\frac{a + b}{a} \right)^d \frac{\cos(\theta_1)}{\cos(\theta_2)} = \frac{R^d}{M^d} \frac{\langle \bar{y} - h_o, x - e_{d+1} \rangle}{\langle o - \bar{y}, e_{d+1} \rangle} \\ &= R^d \left(\frac{\langle \hat{y} - h_o, M\hat{y} + (1 - M)h_o \rangle + \ell_o - \ell_o^2(1 - M)}{M^d \ell_o} \right) \\ &= R^d \left(\frac{M\|\hat{y} - h_o\|^2 + \langle \hat{y} - h_o, h_o \rangle + \ell_o - \ell_o^2(1 - M)}{M^d \ell_o} \right). \end{aligned}$$

For $h_o = 0_d$, $\ell_o = 2$ (Example 2), we have

$$M = \frac{4}{\|\hat{y}\|^2 + 4}$$

and we recover the stereographic projection with Jacobian

$$J_\theta(y) = R^d \frac{1}{M^d} = R^d \left(\frac{\|\hat{y}\|^2 + 4}{4} \right)^d.$$

For $h_o = 0_d$, $\ell_o = 1$ (Example 1), we obtain the Cauchy projection with

$$M = \frac{1}{\sqrt{\|y\|^2 + 1}}$$

and Jacobian

$$J_\theta(y) = R^d \frac{1}{M^d} = R^d \frac{\|\hat{y}\|^2 + 1}{M^{d-1}} = R^d (\|y\|^2 + 1)^{(d+1)/2}.$$

A.2 Proof of Proposition 2

We begin with the following lemma.

Lemma 1. *Given two points x and y on unit sphere $\mathcal{S}^{d+1} \subset \mathbb{R}^{d+1}$, there is a unique greatest circle passing both x and y , which can be written as*

$$c_o(\theta) = \cos(\theta)x + \sin(\theta)u, \quad \theta \in [0, 2\pi),$$

where $u = \frac{y - (x^T y)x}{\sqrt{1 - (x^T y)^2}}$. Suppose the angle between x and y are no larger than $\pi/2$ with $x_{d+1} < \ell_o - 1$ and $y_{d+1} > \ell_o - 1$. The two intersection points of this greatest circle with latitude $\ell_o - 1$ are:

$$p_- := x \cos(\phi - \gamma) + u \sin(\phi - \gamma)$$

which lies on the shorter arc on that greatest circle connecting x and y (aka, spherical linear interpolation or the slerp) and

$$p_+ := x \cos(\phi + \gamma) + u \sin(\phi + \gamma),$$

which lies on the longer complementary arc, and

$$\phi := \arccos \left(\frac{x_{d+1}}{\sqrt{x_{d+1}^2 + u_{d+1}^2}} \right), \quad \gamma := \arccos \left(\frac{\ell_o - 1}{\sqrt{x_{d+1}^2 + u_{d+1}^2}} \right).$$

Proof. For $c_o(\theta)$, one can verify $c_o(0) = x$ and $c_o(\alpha) = x(x^T y) + y - (x^T y)x = y$, where $\alpha := \arccos(x^T y) < \pi/2$ by our assumption. Also, u is a unit vector, as

$$u = \frac{y - (x^T y)x}{\sqrt{1 - (x^T y)^2}} = \frac{y - (x^T y)x}{\|y - (x^T y)x\|}.$$

The two intersection points should satisfy

$$c_o(\theta)_{d+1} = x_{d+1} \cos \theta + u_{d+1} \sin \theta = \ell_o - 1,$$

which gives the solutions $\theta = \phi \pm \gamma$. Finally, the one with $\phi - \gamma$ is on the shorter arc. \square

By Lemma 1, one can easily check that the SCS proposal is symmetric (see Fig. 4 for an illustration) and therefore the detailed balance condition holds for SCS, implying the existence of the stationary distribution π . By [Meyn and Tweedie, 2012, Theorem 13.0.1], Proposition 2 holds if the Markov chain is aperiodic, π -irreducible, and positive Harris recurrent. SCS is aperiodic by [Roberts and Smith, 1994, Theorem 3(i)] using the facts that the acceptance probability does not equal to zero and the proposal distribution as a Markov kernel is aperiodic. Furthermore, π -irreducibility comes from [Roberts and Smith, 1994, Theorem 3(ii)] using the fact that the proposal distribution as a Markov kernel is π -irreducible. Since π is finite, the chain is positive recurrent [Tierney, 1994, pp.1712]. Harris recurrence comes directly from [Tierney, 1994, Corollary 2].

A.3 Proof of Theorem 1

First of all, if $\sup_{y \in \mathbb{R}^d} \pi(y)J(y) = \infty$, SCS is not even geometrically ergodic ([Roberts and Tweedie, 1996, Proposition 5.1]). This implies that the condition in Theorem 1 is necessary. Therefore, it suffices to show $\sup_{y \in \mathbb{R}^d} \pi(y)J(y) < \infty$ is also a sufficient condition.

Recall that \mathcal{S}^{d+1} denotes the unit sphere centered at origin, that is, $\mathcal{S}^{d+1} := \{z \in \mathbb{R}^{d+1} : \sum_{i=1}^{d+1} z_i^2 = 1\}$, and let $\pi_S(z)$ be the transformed target on the unit sphere. Note that when

$\ell_o < 2$, part of the sphere is not used, which we refer to as the “dark side” of the sphere, defined by $\text{DS}(0)$ in the following. We will also define “almost dark side” with size δ , denoted as $\text{DS}(\delta)$. When $\ell_o = 2$, our definition of $\text{DS}(\delta)$ reduces to the definition of “Arctic Circle”, denoted as $\text{AC}(\delta)$, in [Yang et al., 2024, Proof of Theorem 2.1].

1. We define the “dark side” of the sphere as

$$\text{DS}(0) := \{(x, \ell_x - 1) \in \mathcal{S}^{d+1} : \ell_x \geq \ell_o\}.$$

2. Similarly, we can define the “almost dark side” with “size” $\delta \geq 0$ as

$$\text{DS}(\delta) := \{(x, \ell_x - 1) \in \mathcal{S}^{d+1} : \ell_x \geq \ell_o - \delta\},$$

which contains a small area of the boundary of the “bright side” with “size” δ .

3. Same as in [Yang et al., 2024, Proof of Theorem 2.1], we use $\text{HS}(z, 0) := \{z' \in \mathcal{S}^{d+1} : z^T z' \geq 0\}$ to denote the “hemisphere” from z . and $\text{HS}(z, \epsilon') := \{z' \in \mathcal{S}^{d+1} : z^T z' \geq \epsilon'\}$ to denote the area left after “cutting” the hemisphere’s boundary of “size” $\epsilon' \geq 0$.

The rest of the proof is a generalisation of [Yang et al., 2024, Proof of Theorem 2.1], which is a special case for $\ell_o = 2$, to any given $\ell_o \in [1, 2]$. We prove uniform ergodicity by showing the compactification of the “bright side” of the sphere, denoted as $\overline{\text{DS}^c(0)}$, is a small set. More precisely, we will show the 3-step transition kernel satisfies the following minorisation condition:

$$P^3(z, A) \geq \epsilon \pi_S(A), \quad z \in \overline{\text{DS}^c(0)}$$

for all measurable set $A \subset \overline{\text{DS}^c(0)}$, where $\epsilon > 0$. The rationale behind establishing a 3-step minorisation condition is that this facilitates the Markov chain on the sphere being able to reach any point on the “bright side” of the sphere, and there exists enough probability mass around “2-stop” paths to ensure that the chain can avoid stopping too close to the boundary of the “dark side”, the potentially problematic region.

Now we almost completely follow [Yang et al., 2024, Proof of Theorem 2.1]. Consider the 3-step path $z \rightarrow z_1 \rightarrow z_2 \rightarrow z' \in A$ where $z \in \overline{\text{DS}^c(0)}$ is the starting point, z_1 and z_2 are two intermediate points on the sphere, and $z' \in A$ is final point. Denoting $q(z, \cdot)$ as the proposal density, we have

$$p(z, z') \geq q(z, z') \left(1 \wedge \frac{\pi_S(z')}{\pi_S(z)} \right).$$

Then the 3-step transition kernel can be bounded below by

$$\begin{aligned} P^3(z, A) &\geq \int_{z' \in A} \int_{z_2 \in \mathcal{S}^d} \int_{z_1 \in \mathcal{S}^d} q(z, z_1) q(z_1, z_2) q(z_2, z') \\ &\quad \cdot \left(1 \wedge \frac{\pi_S(z_1)}{\pi_S(z)} \right) \left(1 \wedge \frac{\pi_S(z_2)}{\pi_S(z_1)} \right) \left(1 \wedge \frac{\pi_S(z')}{\pi_S(z_2)} \right) \nu(dz_1) \nu(dz_2) \nu(dz') \end{aligned} \tag{8}$$

where $\nu(\cdot)$ denotes the Lebesgue measure on \mathcal{S}^{d+1} .

By the condition we assumed, $\pi(y) > 0$ is continuous in \mathbb{R}^d , which implies $\pi_S(z)$ is positive and continuous in any compact subset of the “bright side” of the sphere $\text{DS}^c(0)$. Then using the fact that a continuous function on a compact set is bounded, if we rule out $\text{DS}(\epsilon)$, $\pi_S(z)$ is bounded away from 0. That is,

$$\inf_{z \notin \text{DS}(\epsilon)} \pi_S(z) \geq \delta_\epsilon > 0, \forall \epsilon \in (0, 1),$$

where $\delta_\epsilon \rightarrow 0$ as $\epsilon \rightarrow 0$.

Furthermore, since the surface area of \mathcal{S}^{d+1} is finite and $\pi_S(z) \propto \pi(y)J(y)$, we know $\sup_{y \in \mathbb{R}^d} \pi(y)J(y) < \infty$ implies that $M := \sup \pi_S(z) < \infty$. Therefore, we have

$$\begin{aligned} P^3(z, A) &\geq \int_{z' \in A} \int_{z_2 \in \mathcal{S}^d \setminus \text{DS}(\epsilon)} \int_{z_1 \in \mathcal{S}^d \setminus \text{DS}(\epsilon)} q(z, z_1)q(z_1, z_2)q(z_2, z') \\ &\quad \cdot \left(1 \wedge \frac{\delta_\epsilon}{M}\right)^2 \left(\frac{\pi_S(z')}{M}\right) \nu(dz_1)\nu(dz_2)\nu(dz'). \end{aligned} \quad (9)$$

Next, we consider the term $q(z, z_1)q(z_1, z_2)q(z_2, z')$. For our algorithm, the proposal can cover the whole hemisphere except the boundary, by “cutting” the boundary a little bit, the proposal density will be bounded below. That is, we have

$$q(z, z') \geq \delta'_{\epsilon'} > 0, \quad \forall z' \in \text{HS}(z, \epsilon'), \epsilon' \in (0, 1),$$

where $\delta'_{\epsilon'} \rightarrow 0$ as $\epsilon' \rightarrow 0$.

Therefore, if $z_1 \in \text{HS}(z, \epsilon')$ and $z_2 \in \text{HS}(z', \epsilon')$ then $q(z, z_1) \geq \delta'_{\epsilon'}$ and $q(z_2, z') \geq \delta'_{\epsilon'}$. Then we have

$$\begin{aligned} &\int_{z_2 \in \text{HS}(z', \epsilon') \setminus \text{DS}(\epsilon)} \int_{z_1 \in \text{HS}(z, \epsilon') \setminus \text{DS}(\epsilon)} q(z, z_1)q(z_1, z_2)q(z_2, z')\nu(dz_1)\nu(dz_2) \\ &\geq (\delta'_{\epsilon'})^3 \int_{z_2 \in \text{HS}(z', \epsilon') \setminus \text{DS}(\epsilon)} \int_{z_1 \in \text{HS}(z, \epsilon') \setminus \text{DS}(\epsilon)} \mathbf{1}_{z_1 \in \text{HS}(z_2, \epsilon')}\nu(dz_1)\nu(dz_2). \end{aligned} \quad (10)$$

Note that as the “bright side” is no smaller than a hemisphere, 3 steps are enough to reach any point z' from any z both on the “bright side”. Furthermore, as the “dark side” of the sphere is no larger than a hemisphere, it is clear that under the Lebesgue measure ν on \mathcal{S}^{d+1} , we can define the following positive constant C :

$$C := \inf_{z, z' \in \text{DS}^c(0)} \int_{z_2 \in \text{HS}(z', 0) \setminus \text{DS}(0)} \int_{z_1 \in \text{HS}(z, 0) \setminus \text{DS}(0)} \mathbf{1}_{z_1 \in \text{HS}(z_2, 0)}\nu(dz_1)\nu(dz_2) > 0.$$

Now consider the following function of $\epsilon \geq 0$ and $\epsilon' \geq 0$

$$C_{\epsilon, \epsilon'} := \inf_{z, z' \in \text{DS}^c(0)} \int_{z_2 \in \text{HS}(z', \epsilon') \setminus \text{DS}(\epsilon)} \int_{z_1 \in \text{HS}(z, \epsilon') \setminus \text{DS}(\epsilon)} \mathbf{1}_{z_1 \in \text{HS}(z_2, \epsilon')}\nu(dz_1)\nu(dz_2).$$

It is clear that $C \geq C_{\epsilon, \epsilon'}$. The difference between them can be bounded by

$$\begin{aligned} C - C_{\epsilon, \epsilon'} &\leq \sup_{z \in \text{DS}^c(0)} \nu(\{z_1 : z_1 \in (\text{HS}(z, 0) \setminus \text{HS}(z, \epsilon')) \cap (\text{DS}(\epsilon) \setminus \text{DS}(0))\}) \\ &\quad + \sup_{z' \in \text{DS}^c(0)} \nu(\{z_2 : z_2 \in (\text{HS}(z', 0) \setminus \text{HS}(z', \epsilon')) \cap (\text{DS}(\epsilon) \setminus \text{DS}(0))\}) \\ &\quad + \sup_{z_2 \in \text{DS}^c(0)} \nu(\{z_1 : z_1 \in \text{HS}(z_2, 0) \setminus \text{HS}(z_2, \epsilon')\}). \end{aligned} \quad (11)$$

Then clearly the upper bound is continuous w.r.t. both ϵ and ϵ' and goes to zero when $\epsilon \rightarrow 0$ and $\epsilon' \rightarrow 0$. Therefore, there exists $\epsilon > 0$ and $\epsilon' > 0$ such that $C - C_{\epsilon, \epsilon'} \leq \frac{1}{2}C$, that is

$$C_{\epsilon, \epsilon'} \geq \frac{1}{2}C > 0.$$

Using such ϵ and ϵ' we have

$$\int_{z_2 \in \text{HS}(z', \epsilon') \setminus \text{DS}(\epsilon)} \int_{z_1 \in \text{HS}(z, \epsilon') \setminus \text{DS}(\epsilon)} q(z, z_1)q(z_1, z_2)q(z_2, z')\nu(dz_1)\nu(dz_2) \geq \frac{1}{2}C(\delta'_{\epsilon'})^3 > 0.$$

Then we have

$$P^3(z, A) \geq \left(1 \wedge \frac{\delta_\epsilon}{M}\right)^2 \frac{1}{2} C(\delta'_\epsilon)^3 \int_{z' \in A} \left(\frac{\pi_S(z')}{M}\right) \nu(\mathrm{d}z')$$

Note that $\pi_S(z') > 0$ almost surely w.r.t. ν if $z' \in \mathrm{DS}^c(0)$. We define

$$g(z') := \begin{cases} \left(1 \wedge \frac{\delta_\epsilon}{M}\right)^2 \frac{1}{2} C(\delta'_\epsilon)^3 \frac{\pi_S(z')}{M}, & \forall z' \in \mathrm{DS}^c(0) \\ 0, & \forall z' \in \mathrm{DS}(0). \end{cases}$$

Note that $g(z) \propto \pi_S(z)$, Hence, we have established

$$P^3(z, A) \geq \int_{z' \in A} g(z') \nu(\mathrm{d}z') \geq \epsilon \pi_S(A),$$

where $\epsilon = \left(1 \wedge \frac{\delta_\epsilon}{M}\right)^2 \frac{1}{2} C(\delta'_\epsilon)^3 \frac{1}{M} > 0$. This established the desired minorisation condition and completed the proof.

A.4 Choice for the latitude ℓ_o

The variational method presented in Section 3 applies for a fixed latitude $\ell_o \in [1, 2)$, as the support of the density on the bright side depends on this parameter. Our choice of ℓ_o is guided by simple geometric properties of the hyper-sphere in high dimensions. For $o \in \mathcal{B}^{d+1}(e_{d+1})$, let

$$\mathcal{D}_o^{d+1} = \mathcal{S}^{d+1}(e_{d+1}) \setminus \mathcal{C}_o^{d+1} = \{x \in \mathbb{R}^{d+1} : \|h_x\|^2 + (\ell_x - 1)^2 = 1; \ell_x \geq \ell_o\}$$

be the dark side of the sphere surface, that is removed in the SCP. The following result shows that the removed surface region has asymptotically negligible surface area compared to the sphere surface, when $\ell_o \geq 1 + \mathcal{O}(\log d / \sqrt{d})$.

Proposition 3. *For any $d \geq 1$ and $\ell_o \in (1, 2)$,*

$$\frac{|\mathcal{D}_o^{d+1}|}{|\mathcal{S}^{d+1}|} \leq \frac{e^{1/2}}{2} \sqrt{d+1} \left[1 - (\ell_o - 1)^2\right]^{\frac{d-1}{2}}, \quad (12)$$

where $|\cdot|$ is the d -dimensional surface area.

Proof. Let X and Y be independent chi-square random variables with d and 1 degrees of freedom, respectively. Using the fact that the surface area ratio can be written as an angle ratio, we are interested in the probability

$$\frac{\text{surface area of "dark side"} }{\text{surface of the sphere}} = \mathbb{P}\left(X \leq \frac{1 - (\ell_o - 1)^2}{(\ell_o - 1)^2} Y\right).$$

We first start with the exact formula of $\mathbb{P}(X \leq cY)$, for some constant c . Using the F -distribution, we have $\frac{X/d}{Y/1} \sim F_{d,1}$ which implies

$$\mathbb{P}(X < cY) = \mathbb{P}\left(\frac{X}{Y} < c\right) = \mathbb{P}(dF_{d,1} < c) = \mathbb{P}\left(F_{d,1} < \frac{c}{d}\right) = F_F\left(\frac{c}{d}; d, 1\right),$$

where $F_F(x; d, 1)$ denotes the c.d.f. function of an F -distribution with $(d, 1)$ degrees of freedom. The c.d.f. of the F -distribution can be written in terms of the regularized incomplete beta function:

$$F_F(x; d, 1) = I_{\frac{d x}{d x + 1}}\left(\frac{d}{2}, \frac{1}{2}\right),$$

where $I_z(a, b) = \frac{1}{B(a, b)} \int_0^z t^{a-1} (1-t)^{b-1} dt$. Substituting $x = \frac{c}{d}$ yields the exact formula:

$$\mathbb{P}(X < cY) = I_{\frac{d(c/d)}{d(c/d) + 1}}\left(\frac{d}{2}, \frac{1}{2}\right) = I_{\frac{c}{c+1}}\left(\frac{d}{2}, \frac{1}{2}\right).$$

Next, we derive an upper bound for large enough dimension d . By Markov's inequality, for any $t > 0$ such that the moment generating functions exist,

$$\mathbb{P}(X < cY) = \mathbb{P}(e^{-tX} \geq e^{-tcY}) \leq \mathbb{E}[e^{-tX+tcY}] = M_X(-t) M_Y(tc).$$

For $Z \sim \chi_k^2$, the moment generating function is

$$M_Z(u) = (1 - 2u)^{-k/2}, \quad u < \frac{1}{2}.$$

Hence, for $0 < t < 1/(2c)$,

$$\mathbb{P}(X < cY) \leq (1 + 2t)^{-d/2} (1 - 2ct)^{-1/2}.$$

Choosing $t^* = \frac{d-c}{2c(d+1)}$, one obtains the tightest bound of that form

$$\mathbb{P}(X < cY) \leq \left(1 + \frac{1}{c} \frac{d-c}{d+1}\right)^{-d/2} \cdot \left(1 - \frac{d-c}{d+1}\right)^{-1/2} = \sqrt{\frac{d+1}{1+c}} \left[\frac{d+1}{d} \cdot \frac{c}{c+1}\right]^{d/2}.$$

Using $(1 + 1/d)^d < e$, we have

$$\mathbb{P}(X < cY) \leq \sqrt{\frac{d+1}{c+1}} e^{1/2} \left(\frac{c}{c+1}\right)^{d/2} = \sqrt{d+1} e^{1/2} \sqrt{\frac{1}{c+1} \left(1 - \frac{1}{c+1}\right)} \left(\frac{c}{c+1}\right)^{\frac{d-1}{2}}.$$

Since $\sqrt{\frac{1}{c+1} \left(1 - \frac{1}{c+1}\right)} \leq \frac{1}{2}$, we have

$$\mathbb{P}(X < cY) \leq \frac{e^{1/2}}{2} \sqrt{d+1} \left(\frac{c}{c+1}\right)^{\frac{d-1}{2}}.$$

Finally, substituting $c = \frac{1-(\ell_o-1)^2}{(\ell_o-1)^2}$ gives the desired result. \square

Proposition 3 implies that, by restricting $\ell_o \in (1 + \frac{c}{\sqrt{d}}, 2)$, with $c \sim \log d$ the ratio (12) shrinks fast as the dimension increases, making increasingly unlikely for the SPS proposal to land on the dark side. However, for Cauchy distributions, Example 1 shows that the optimal choice corresponds to $\ell_o = 1$. In practice, we found $\ell_o = 1.1$ to be a reasonable choice in all our simulations, and we leave for future work the fine tuning of this parameter.

A.5 Slow mixing of DA-Gibbs

For Bayesian logistic regression, it has been noticed that DA-Gibbs also performs poorly when the two classes are imbalanced. Johndrow et al. [2019] studied the mixing behavior of DA-Gibbs in the infinitely imbalanced asymptotic regime introduced by Owen [2007]. Johndrow et al. [2019] argue that the slow mixing is due to the discrepancy between the width of the posterior and the step-size of Gibbs (the step-size converges to 0 at a faster rate than the concentration of the posterior as the sample size $n \rightarrow \infty$). We notice a similar phenomenon when the two classes are perfectly separable, providing an explanation for the poor performance of DA-Gibbs in the empirical results of Ghosh et al. [2018].

Consider a one-dimensional logistic regression with student t prior with ν degrees of freedom

$$\mathbb{P}(Y_i = 1 \mid \beta) = \sigma(x_i \beta), \quad \sigma(t) = \frac{1}{1 + e^{-t}}$$

and assume the following separable data

$$(x_i, y_i) = \begin{cases} (n^{-1/2}, 1) & i \leq n/2 \\ (-n^{-1/2}, 0) & i > n/2 \end{cases}$$

for $i = 1, 2, \dots, n$. In the Gibbs sampler, the student t prior $t_\nu(0, \tau^2)$ is represented as a scale-mixture of Gaussians:

$$\beta \mid \lambda \sim N\left(0, \frac{\tau^2}{\lambda}\right), \quad \lambda \sim \text{Gamma}\left(\frac{\nu}{2}, \frac{\nu}{2}\right),$$

and Pólya-Gamma latent variables are used for the logistic link [Polson et al., 2013].

Define the rescaled coefficient $\eta = \beta/\sqrt{n}$. In the η -parameterization, the log likelihood is

$$\log p(y \mid \eta) = \frac{n}{2} \log \sigma(\eta) + \frac{n}{2} \log(1 - \sigma(-\eta)) = n \log \sigma(\eta),$$

and the derivative w.r.t. η is

$$\frac{\partial}{\partial \eta} \log p(y \mid \eta) = n\sigma(-\eta).$$

The Student t prior in β induces the prior in η :

$$\pi_\eta(\eta) \propto \left(1 + \frac{n\eta^2}{\nu\tau^2}\right)^{-(\nu+1)/2}.$$

Moreover, we have

$$\frac{\partial}{\partial \eta} \log \pi_\eta(\eta) = -\frac{(\nu+1)n\eta}{\nu\tau^2 + n\eta^2}.$$

Combining the likelihood and prior, the derivative of the log posterior is given by

$$\frac{\partial}{\partial \eta} \log p(\eta \mid y) = n\sigma(-\eta) - \frac{(\nu+1)n\eta}{\nu\tau^2 + n\eta^2}.$$

We now study the scale of the posterior standard deviation and the scale of the step-size in β for large n .

- **Scale of posterior width.** We first argue that, for large n , the posterior standard deviation in η is of order $O(\sqrt{\log n})$. For large η , $\sigma(-\eta) \sim e^{-\eta}$ and $\frac{\partial}{\partial \eta} \log \pi_\eta(\eta) \sim -\frac{\nu+1}{\eta}$, so the mode $\hat{\eta}_n$ solves

$$ne^{-\hat{\eta}_n} \sim \frac{\nu+1}{\hat{\eta}_n} \implies \hat{\eta}_n \sim \log n.$$

Differentiating again at the mode gives

$$-\frac{\partial^2}{\partial \eta^2} \log p(\eta \mid y) \sim n\sigma(-\hat{\eta}_n) + \frac{\nu+1}{\hat{\eta}_n^2} \sim \frac{\nu+1}{\hat{\eta}_n} = O\left(\frac{1}{\log n}\right).$$

Hence, the posterior standard deviation in η is about $O(\sqrt{\log n})$. In terms of β , the posterior standard deviation is of order $O(\sqrt{n \log n})$.

- **Scale of step-size.** In the Pólya-Gamma Gibbs sampler [Polson et al., 2013], the Pólya-Gamma variables ω_i have the conditional distribution

$$\omega_i \mid \eta \sim \text{PG}(1, x_i \beta) = \text{PG}(1, \pm \eta),$$

with mean given by

$$\mathbb{E}[\omega_i \mid \eta] = \frac{1}{2|\eta|} \tanh\left(\frac{|\eta|}{2}\right) \sim \frac{1}{2|\eta|} \quad (|\eta| \rightarrow \infty).$$

Moreover, the conditional variance of β given the Pólya-Gamma variables is given by

$$\text{Var} [\beta \mid \omega] = \left(X^\top \Omega X + \tau^{-2} \lambda\right)^{-1}.$$

Note that $X^\top \Omega X = \sum_i \omega_i x_i^2 = \frac{1}{n} \sum_i \omega_i$. Near the mode of η , we have $\mathbb{E}[\omega_i \mid \eta] \sim \frac{1}{2\log n}$. Thus $X^\top \Omega X \sim \frac{1}{2\log n}$. Because $\lambda \mid \beta \sim \text{Gamma}\left(\frac{\nu+1}{2}, \frac{\nu+\beta^2/\tau^2}{2}\right)$, we have $\mathbb{E}[\lambda \mid \beta] = \frac{\nu+1}{\nu+\beta^2/\tau^2}$. Near the posterior mode, $\beta^2 \sim n(\log n)^2$, thus $\lambda/\tau^2 \sim \frac{1}{n(\log n)^2}$ is negligible compared to $X^\top \Omega X$. So we have

$$\text{Var}[\beta \mid \omega] \sim (X^\top \Omega X)^{-1} \sim \log n,$$

which means the step-size in β is of order $O(\sqrt{\log n})$.

In summary, the posterior width in β is $O(\sqrt{n \log n})$, but the Pólya-Gamma Gibbs step-size in β is $O(\sqrt{\log n})$. The step-size is smaller than the posterior width by a factor of \sqrt{n} , causing slow mixing of the Gibb sampler.